[논 문] 한국재료학회지
Korean J. Mater. Res.
Vol. 31, No. 5 (2021)

https://doi.org/10.3740/MRSK.2021.31.5.255

An Empirical Approach to Analyze Creep Rupture Behavior of P91 Steel

Muhammad Junaid Aslam[1†] and Cemil Hakan Gur[1,2]

[1]Department of Metallurgical and Materials Engineering, Middle East Technical University, Ankara, Turkey
[2]Welding Technology and NDT Research/Application Center, Middle East Technical University, Ankara, Turkey

(Received March 11, 2021 : Revised April 12, 2021 : Accepted April 21, 2021)

Abstract P91 steel has been a highly researched material because of its applicability for high-temperature applications. Considerable efforts have been made to produce experimental creep data and develop models for creep life prediction. As creep tests are expensive and difficult to conduct, it is vital to develop authenticated empirical methods from experimental results that can be utilized for better understanding of creep behavior and can be incorporated into computational models for reliable prediction of creep life. In this research, a series of creep rupture tests are performed on the P91 specimens within a stress range of 155 MPa to 200 MPa and temperature range of 640 °C (913 K) to 675 °C (948 K). The microstructure, hardness, and fracture surfaces of the specimens are investigated. To analyze the results of the creep rupture tests at a macro level, a parameter called creep work density is derived. Then, the relationships between various creep parameters such as strain, strain rate, time to rupture, creep damage tolerance factor, and creep work density are investigated, and various empirical equations are obtained.

Key words P91 Type 2 steel, creep life, creep damage, creep work density, strain energy density.

1. Introduction

Creep is the dominant damage mechanism for the critical components operating under static load at high temperatures. P91 type steels (9Cr1Mo) with optimum addition of some precipitate forming elements have been widely applied as pipework components working at temperatures between 370 °C to 650 °C.[1)] After the development of the first alloy corresponding to P91 steel in late 1970s.[2-5)] considerable research effort have been performed to explore its metallurgical and mechanical properties.[6-10)]

The microstructure of the as-received material, operating temperature, applied stress, size of prior austenite grains, and martensite lath packets, size, and amount of precipitates are the main factors that affect the creep rupture strength of P91 steel. Generally, P91 steel is produced by normalizing (1,040-1,080 °C) and tempering (750-780 °C), which results in a dislocation-rich microstructure consisting of tempered martensite with M23C6 carbides, and V/Nb rich MX-type precipitates.[11-13)] The minimum mechanical properties of P91 steel at room temperature are the yield strength of 415 MPa, tensile strength of 585 MPa, and 20% elongation in length as per latest ASTM standard A335/A335M.[14)]

To operate over extremely long time periods, it is critical to estimate the allowable stress accurately within the operating temperature range. The creep stress range for P91 steel is defined depending on the temperature; for instance, the high-stress range is 130-200 MPa at 600 °C, whereas it is around 70-100 MPa at 650 °C.[15-17)] According to the ASME Boiler and Pressure Vessel Code, steel selection for power plant applications is based on the allowable creep strength, calculated from the tensile stresses that can be sustained without failure in 100,000 hours (h) at the operating temperatures.[1)] Based on the creep test data analysis, the 100,000 h strength of the P91 steel at 600 °C has been estimated as 85 MPa.[9)] Further, P91 welded components are permitted to be used at 370 °C for the creep stress levels of 155 MPa and 183 MPa for engineering components of ASME sections I (Power Boiler parts), III (Nuclear parts)

†Corresponding author
E-Mail : e195211metu@gmail.com (M. J. Aslam, METU, Ankara)

& VIII (pressure vessel parts) respectively.[1)]

Long service exposure degrades the creep properties of P91 steel due to modification and softening of the microstructure via extensive recovery of the lath and dislocation structure together with carbide coarsening.[11,12,18)] F, Vivier have examined the microstructure of P91 after long-term exposure at 600 °C and a short-term exposure at 500 °C.[11)] After about 113,000 h exposure at 600 °C, Cr-rich M23C6 carbides, MX-type precipitates, Laves phase, and a small amount of modified Z phase were observed with a decrease in microhardness; however, no remarkable variation in micro-hardness and precipitates were noted after about 4300h exposure at 500 °C.

There have been research efforts to produce data for P91 steel by performing creep tests and to develop the creep life prediction models. Since conducting creep tests is expensive in terms of time consumption and cost, it is necessary to establish legitimate empirical methods, which can provide the empirical basis for computational models' enhancements and trustworthy creep rupture time estimations.[19-21)] In the present investigation, creep rupture tests were performed systematically for the stress and temperature variations of 155 MPa to 200 MPa, and of 640 °C (913K) to 675 °C (948K) correspondingly.

2. Classical Empirical Relations During Creep Regime

A typical CRT curve consists of well-defined zones, and it directly yield's various empirical parameters like instantaneous strain (ε_o), strain gain during primary region (ε_I), strain gain during secondary region (ε_{II}), time gain during primary region (t_{II}), minimum or steady-state strain rate in secondary creep region ($\dot{\varepsilon}_{II}$), strain gain during tertiary region (ε_{III}), time gain during tertiary region (t_{III}), rupture strain (ε_r), and average strain rate ($\dot{\varepsilon}_{avg}$) as illustrated in Fig. 1.

Based on the continuum creep damage mechanics, that defines the relationship between creep straining and rupture phenomenon,[22)] a dimensionless creep damage tolerance factor (λ) has been developed by Dyson and Leckie.[23-25)] They have evoked that λ gives a meaningful way of creep ductility quantification by taking into account the localized necking and cracking vulnerability by the empirical relation as follows.

$$\lambda = \left(\frac{\varepsilon_r}{\dot{\varepsilon}_{II} \cdot t_r}\right) = \frac{\dot{\varepsilon}_{avg}}{\dot{\varepsilon}_{II}} \tag{1}$$

Although $\dot{\varepsilon}_{avg}$ is utilized in determining the creep damage tolerance factor (λ), however, it is seldom discussed as a individual parameter in creep tests. Furthermore, ε_r results from the noteworthy contributions of steady-state rate and tertiary creep rate, likewise $\dot{\varepsilon}_{avg}$. Henceforth, $\dot{\varepsilon}_{avg}$ can be identified as one of the parameters which determine the level of balance between the primary creep rate, steady-state creep rate and tertiary creep rate as shown in a classical creep curve (Fig. 1).

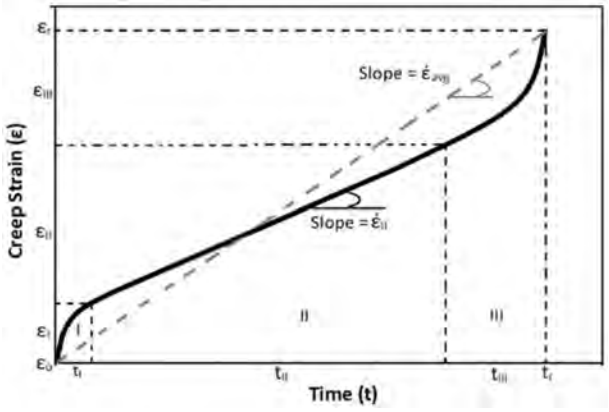

Fig. 1. Schematical presentation of the creep curve.

3. Contemporary Creep Energy Empirical Relations

The creep failure is directly dependent upon the absorbed internal energy density, thus, at macroscopic level the energy dissipated in the component can be taken as a measure of creep rupture. The strain energy density required to cause rupture in the creep rupture test [J·mm^{-3}] can be defined using eq. (2).

$$E_c = \int_0^{t_r} \sigma_{ij}\, \dot{\varepsilon}_{ij}\, dt \tag{2}$$

This is further modified by splitting for an individual CRT region by eq. (3) as follows.

$$\begin{aligned} E_c &= E_0 + E_I + E_{II} + E_{III} \\ &= \sigma \left[\varepsilon_o + \int_0^{t_1} \dot{\varepsilon}_I(t) \cdot dt + \dot{\varepsilon}_{II} \cdot \int_{t_1}^{t_2} dt + \int_{t_2}^{t_r} \dot{\varepsilon}_{III}(t) \cdot dt\right] \end{aligned} \tag{3}$$

where 0, I, II, and III refer to instantaneous, primary, steady-state (secondary) and tertiary creep regions. Since the average strain rate address the rate of strain rates during all of the three regions, so the strain energy density equation is further simplified by the substitution of average strain rate as in eq. (4),

$$E_c = \sigma \cdot \dot{\varepsilon}_{avg} \cdot t_r = \sigma \cdot \varepsilon_r \tag{4}$$

Further, the creep work density is derived from eq. (4) as demonstrated in eq. (5).

$$W_c = E_c \cdot t_r = \sigma \cdot \varepsilon_r \cdot t_r \tag{5}$$

Using a similar approach, the work density for the steady-state creep stage [J·h·mm^{-3}] can be calculated via eq. (6).

$$W_{II} = E_{II} \cdot \Delta t_{II} = \sigma \cdot \varepsilon_{II} \cdot \Delta t_{II} \quad (6)$$

Reliable estimation of creep behavior is critical in high temperature plant operations, with creep acting as a dominant failure mechanism limiting the useful life of the components. An empirical parameter called creep work density has been developed, and extents of the average strain rate, steady state strain rate, and creep damage tolerance factor were estimated. The disclosed empirical relations, especially the novel "creep work density" parameter are a valuable contribution towards the understanding of creep behavior from the energy approach.

4. Experimental

The test specimens were prepared from the as-received P91 steel pipe i.e., from base metal. The chemical composition requirements according to ASTM A335/A335M−19a,[14] and the results of the spectroscopic analysis are given in Table 1. The chemical composition of the pipe material[26] lies within the compositional ranges of the P91 Type 2.

The plates with dimensions of 140 mm × 200 mm were extracted from the raw material in pipe form with the aid of conventional machining operations. The plates were heated at 1,050 °C for half an hour, and air-cooled to room temperature; then, subjected to tempering heat treatment at 780 °C for 2 h.

A series of the creep rupture tests (CRT) were performed (see Table 2). The specimens, having a gauge length of 30 mm, and a gauge diameter of 6 mm, were prepared according to ASTM E 139.[27] The stress values for CRT were chosen by considering the minimum (155 MPa) and the maximum allowed (183 MPa) values for P91 steels in ASME BPV Code sections I, III, and VIII.[1] The yield strength values of P91 steel at 25 °C, 640 °C and 675 °C are 415 MPa, 275 MPa, and 265 MPa as per ASME Section II[1] respectively. Thus, the stress level used in all CRTs is below the yield strength of the material.

Table 2. CRT parameters and designation of the specimens.

CRT parameters		Specimen Designation
Stress (MPa)	Temperature (°C)	
155	650	S155-T650C
155	675	S155-T675C
185	640	S185-T640C
200	640	S200-T640C
200	659	S200-T650C

Microstructure investigations were performed using SEM. The specimens were prepared via conventional metallographic procedure, and then, etched with the 10 % Nital reagent. Hardness values of the specimens before and after CRT were measured in the HV0.1 scale.

5. Results and Discussion

The microstructure investigations confirm the achievement of the tempered martensitic microstructure with some precipitates (M23C6, MX, and Nb-V types). Representative SEM macrographs for the specimens having the longest CRT duration (S155-T650C) and the shortest CRT duration (S200-T650C) are illustrated in Fig. 2. They show that there is a negligible microstructural degradation during CRT. Moreover, the precipitates are distributed homogenously within grains and at the Grain boundaries. The hardness values given in Table 3 indicate little softening impact of CRT. The representative fractographs of the same specimens given in Fig. 3 confirm the negligible microstructural degradation. The fracture surfaces have a clear ductile fracture appearance with the presence of dimples. The presented results are in good agreement with the studies of Vivier et al.,[11] who have observed the ductile rupture mechanisms under high-stress levels for P91 steel from 500 °C to 600 °C.

The creep rupture test (CRT) graphs of the specimens are given in Fig. 4, which are in line with the literature.[28]

Table 1. Chemical composition.

Material	Chemical Composition (wt.%)										
	C	Mn	S	Si	Cr	Mo	B	Ni	Cu	As	Others
P91-Type 1 (A335/A335M−19a)	0.08-0.12	0.3-0.6	0.01	0.2-0.5	8-9.5	0.85-1.85	*NS	0.4 (max)	*NS	*NS	Nb = 0.06-0.1; V = 0.18-0.25; N = 0.03-0.07; P = 0.02; Al = 0.02
P91-Type 2 (A335/A335M−19a)	0.08-0.12	0.3-0.5	0.005	0.2-0.4	8-9.5	0.80-1.85	0.001 (max)	0.2 (max)	0.1 (max)	0.01	Nb = 0.06-0.1; V = 0.18-0.25; N = 0.03-0.07; P = 0.02; Al = 0.02
P91 specimens (Spectro. Analysis)	0.1	0.4	0.004	0.3	8.6	0.9	0.0008	0.16	0.02	0.01	Nb = 0.08, V = 0.25; N = 0.05, Al = 0.002; P = 0.14

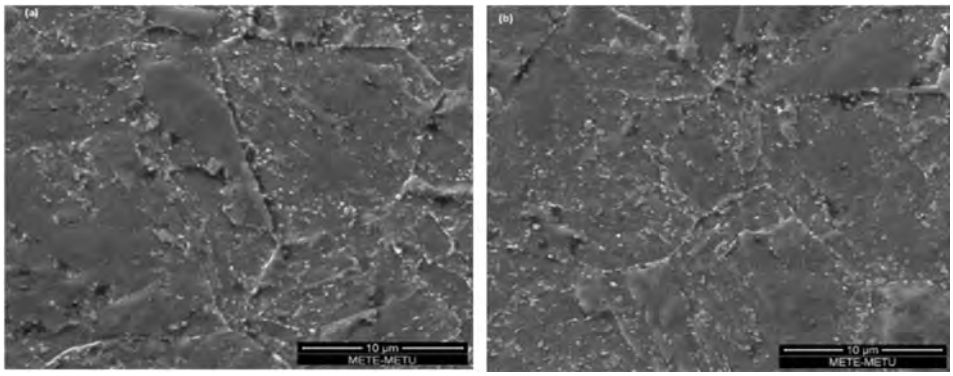

Fig. 2. SEM micrographs of the specimens : (a) S155-T650C, (b) S200-T650C.

Table 3. Hardness values of CRT specimens before and after the creep rupture tests.

	S155-T650C	S155-T675C	S185-T640C	S200-T640C	S200-T650C	Avg. Hardness
Before CRT	243	238	240	239	237	239 ± 2 HV
After CRT	223	217	224	227	229	224 ± 4 HV

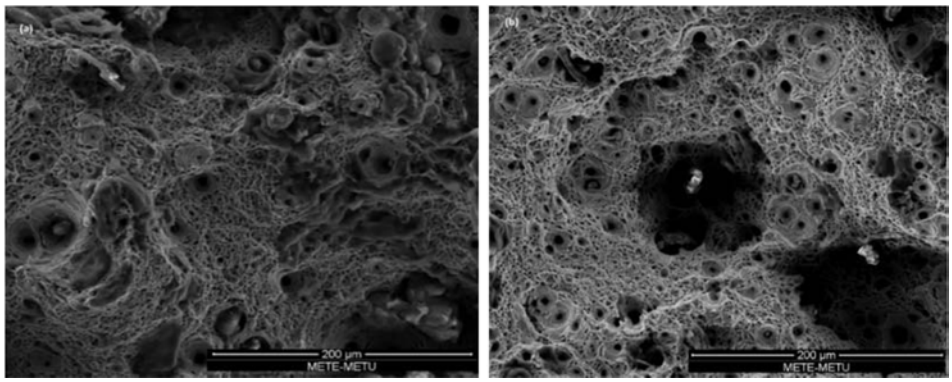

Fig. 3. SEM images of the specimens: (a) S155-T650C, (b) S200-T650C.

All creep curves have a negligible strain gain on the instantaneous application of the stress (ε_o), minor primary region (ε_I), sound secondary, i.e., steady-state region (ε_{II}), and tertiary region (ε_{III}). The minor primary creep region attributes to no microstructure degradation and also constant dislocation density due to short duration of creep tests. Figs. 4(a) and (b) show the effect of the increase in stress at constant temperature whereas Figs. 4(c) and (d) show the effect of the increase in temperature at constant stress on the creep behavior. Rupture time decreased with the increasing temperature and applied stress.

Fig. 5(a) shows the distribution of percentage strain corresponding to each creep stage in the CRT diagram. The percent ε_{II} ($\%\varepsilon_{II}$) is less than percent ε_{III} ($\%\varepsilon_{III}$) for all CRT's, thus it indicates that the contribution of homogeneous deformation in the steady-state creep stage is less than the localized deformation in the tertiary creep stage. However, the contribution level of the steady-state creep increases as stress and temperature decrease. Such a contribution of $\%\varepsilon_{II}$ and $\%\varepsilon_{III}$ have also been reported by Nassif et al.[29] Fig. 5(b) demonstrates the correlations between $\%\varepsilon_{II}$ and $\%\varepsilon_{III}$ with rupture time. The $\%\varepsilon_{II}$ exhibits a direct relation to the rupture time whereas $\%\varepsilon_{III}$ exhibits an inverse relationship. Moreover, the slight slope of these trends shows the linearity of these variations.

Fig. 6(a) shows the distribution of % time spent corresponding to each creep stage in the CRT diagram whereas Fig. 6(b) demonstrates the correlation between the rupture time and the time spent in the steady-state region. The time consumed in the steady-state creep stage is relatively higher than the time spent in the tertiary creep stage, i.e., percent straining in the steady-state zone is more challenging to attain than in the tertiary zone.

Based on the developed correlation between the rupture time and time spent during the steady-state creep in Fig. 6(b), further extrapolated to eq. (7).

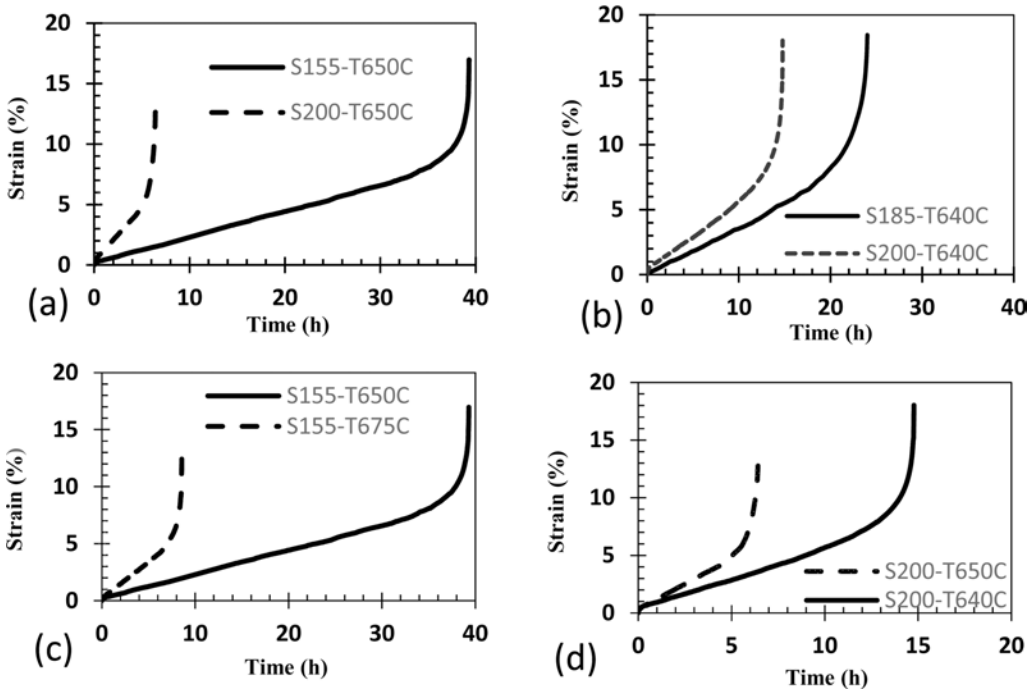

Fig. 4. CRT curves (a) S155-T650C and S200-T650C, (b) S185-T640C and S200-T640C, (c) S155-T650C and S155-T675C, (d) S200-T640C and S200-T650C.

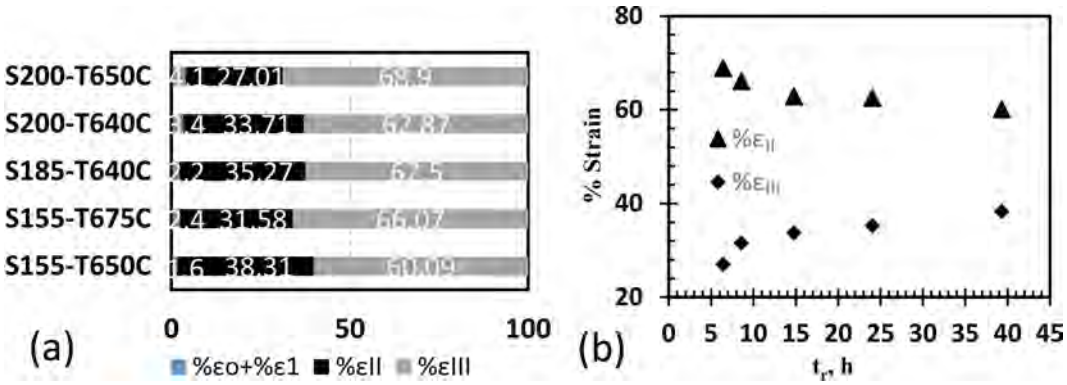

Fig. 5. (a) Percent strain values corresponding to each creep stage in the CRT diagram, (b) Correlations between percent steady-state creep strain ($\%\varepsilon_{II}$), percent tertiary creep strain ($\%\varepsilon_{III}$) and rupture time (t_r).

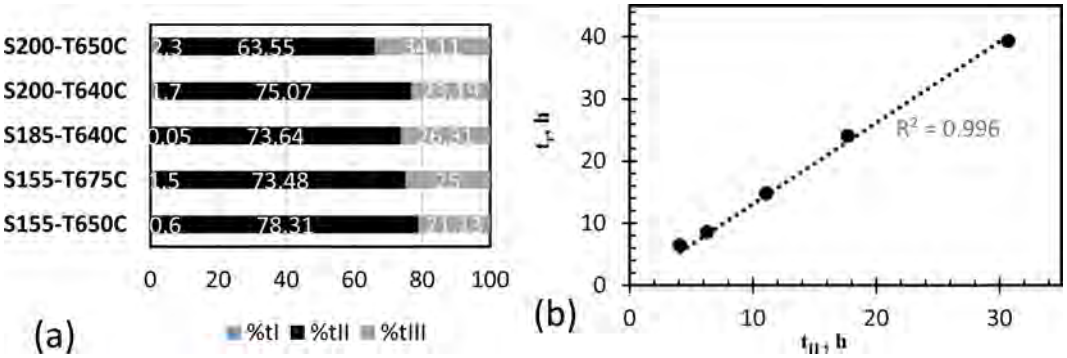

Fig. 6. (a) Percent time spent corresponding to each creep stage in the CRT diagram; (b) Correlation between the rupture time (t_r) and the time spent in the steady-state region (t_{II}).

$$t_r = \alpha \cdot t_{II} \quad (7)$$

Where, α refers to steady state time equation constant which is dependent upon the stress and temperature. For this particular study in the ranges of 155-200 MPa and 640-675 °C, α is found to be 1.31 from the slope of figure 6(b).

The results of the present research, i.e., high $\%\varepsilon_{III}$ and less $\%\varepsilon_{II}$ accompanying in less $\%t_{III}$ and high $\%t_{II}$, can be used for the validation and improvement of creep analytical models. For instance, Nassif et al.[29] has developed a creep model for estimating the tertiary creep and creep rupture phenomena in ferritic/martensitic steels. In the algorithmic aspects of microstructure modeling, the average domain strain rate values have been estimated individually for the different creep- microstructure phenomena. Since the tertiary creep region is initiated by the cavity nucleation and accompanied with the cavity growth, the tertiary creep strain evaluated demonstrates the growth of cavities at the exponential rate. The experimental results presented in Fig. 6 can be used for the endorsement and amendment of creep life prediction algorithms. Similarly, Choudhary et. al.[30] has stated the influence of $\%\varepsilon_{III}$ similar to this research's findings and hence also valid for $\%\varepsilon_{II}$.

Fig. 7(a) demonstrates the weightage difference of $\dot{\varepsilon}_{avg}$ and $\dot{\varepsilon}_{II}$. The $\dot{\varepsilon}_{avg}$ have not evaluated empirically as an individual parameter before for the CRT's of this material, which contribute to one of the unique approaches of this research; however, $\dot{\varepsilon}_{II}$ is a well-researched parameter, and its trend is in harmony with the previous findings,[31,32] i.e., the decrement of $\dot{\varepsilon}_{II}$ at 600 °C is illustrated with the decreasing creep stress values during high stress,[30] and the low-stress regime,[33] respectively, for the P91 steels. Falling creep stress values result in the rise of t_r values for the constant creep temperature.[30,33] The $\dot{\varepsilon}_{II}$ data obtained from current work presented together with the Whilshire et al. data at identical temperature i.e., 650 °C,[17] the results of the current research are found to be consistent, as shown in Fig. 7(b). The correlation between t_r and $\dot{\varepsilon}_{II}$, as illustrated in Fig. 8, can be expressed in the form of a power equation [eq. (8)].

$$t_r = A\ (\dot{\varepsilon}_{II})^n \quad (8)$$

where A refers to a creep equation constant which is dependent upon the stress and temperature. For the ranges of 155-200 MPa and 640-675 °C, A is found to be approximately 5 and n is about -3/2. The $\dot{\varepsilon}_{II}$ graphs drift with t_r for the specimens are in line with the previous literature,[17,34,35] which demonstrates the inverse logarithmic relation.

Relationship between $\dot{\varepsilon}_{avg}$ and $\dot{\varepsilon}_{II}$, as illustrated in Fig. 9, can be expressed in linear form eq. (9).

$$\dot{\varepsilon}_{avg} = \beta\ \dot{\varepsilon}_{II} \quad (9)$$

where β refers to the strain rate equation constant which is dependent upon the stress and temperature. For the series of experiments of this study, i.e., for the ranges of 155-200 MPa and 640-675 °C, β is found to be around 2. Hence, this relation leading to the worth mentioned conclusion that $\dot{\varepsilon}_{avg}$ is increased at least by the factor of

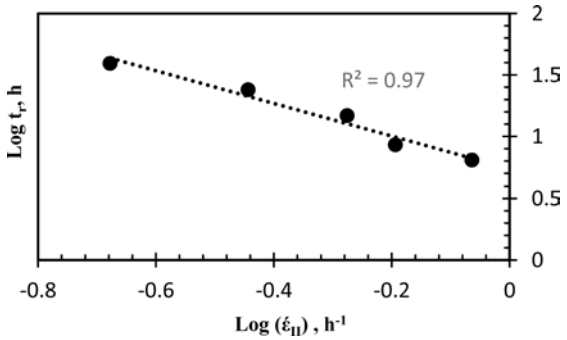

Fig. 8. Correlation between the rupture time and the steady-state strain rate.

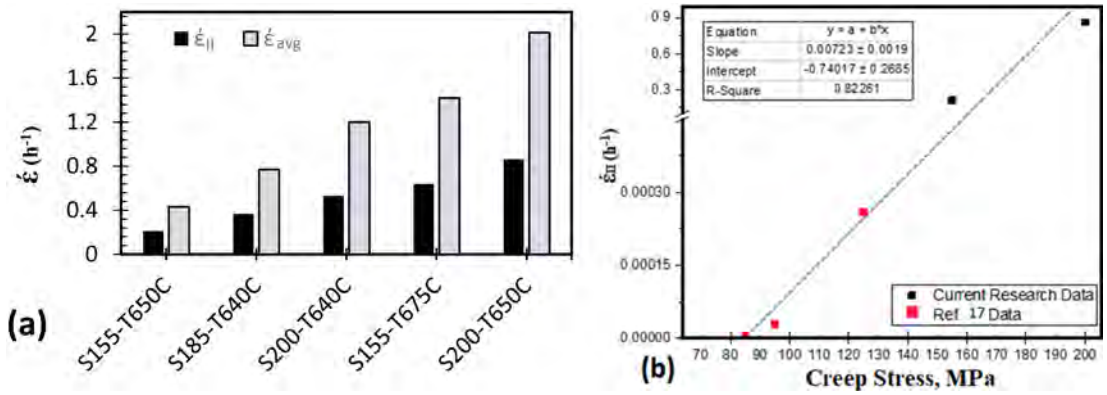

Fig. 7. (a) Average and steady-state strain rate values of the specimens, (b) Correlation between the steady-state creep rate ($\dot{\varepsilon}_{II}$) and creep stress for the data from current research and Ref. [17] at 650 °C.

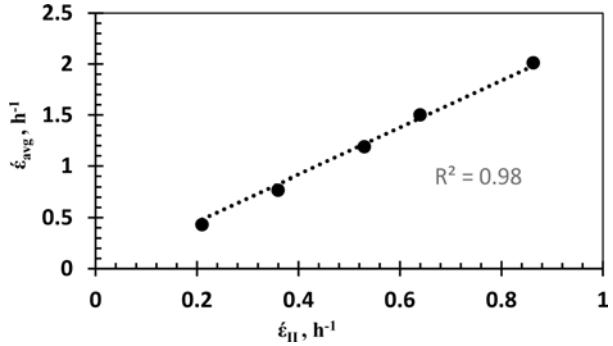

Fig. 9. Correlation between steady-state strain rate ($\dot{\varepsilon}_{II}$) and average strain rate.

two times of the $\dot{\varepsilon}_{II}$, irrespective of the percentage change in t_r.

The work density values of the specimens corresponding to the total creep work density (W_C) and to the steady-state creep stage (W_{II}) are presented in Figs. 10(a) and 10(b). It is found to be possessing high value for the low temperatures than high temperatures for every creep stress value. This trend shows less energy expenditure per unit volume at high creep temperatures resulting in lesser creep strengths in terms of shorter creep life. Likewise, Fig. 11(a) is validating this fact for the stress and temperature range of this research. It also correspondingly validates the reduction of %ε and strain-rate increment at

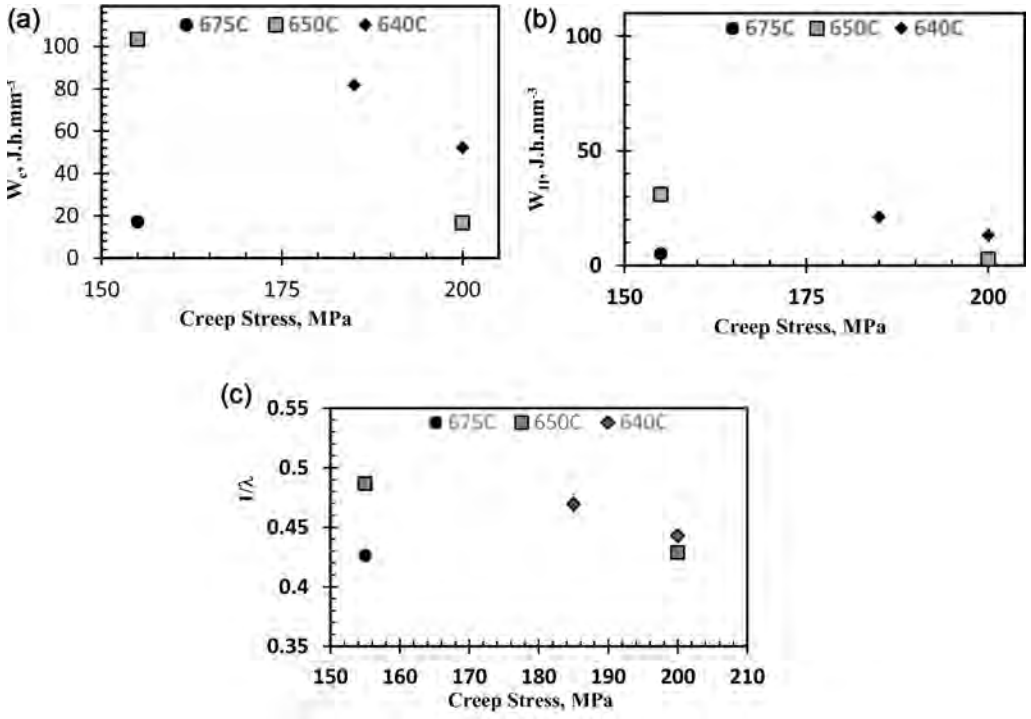

Fig. 10. (a) Relation between creep work per unit volume, stress and temperature, (b) Relation between steady-state creep work per unit volume, stress and temperature, (c) Relation between creep damage tolerance factor, stress, and temperature.

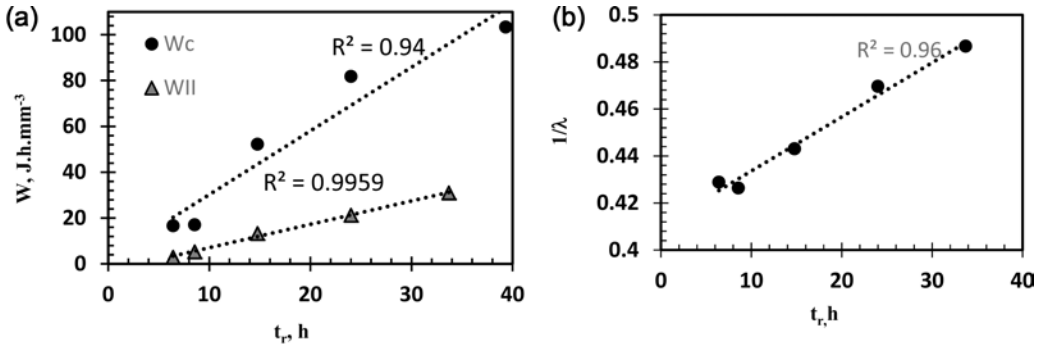

Fig. 11. (a) The relation between the total creep work density, the steady-state creep work density and the rupture time, (b) Relation between the inverse of the creep damage tolerance factor and the rupture time.

high temperatures in comparison to those at lower test temperatures under the effect of identical stress value.

Remarkably, the trend of W_C and W_{II} is similar to the reciprocal of λ (the creep damage tolerance factor) as shown in Figs. 10(a), (b), and (c). Even so, the W_C and W_{II} relationship demonstrate that the creep life is governed by the creep strain accumulation, i.e., the failure mechanisms are strain-controlled, which is also authenticating the work of Wilshire.[17,22] The CDTF (l) values presented in Fig. 10(c) were calculated from an empirical approach i.e., via eq. (1). Moreover, λ follows a similar arrangement as for $\acute{\varepsilon}_{II}$, i.e., λ attained the high values for high temperatures than low temperatures at all creep stress values. The similarity of these patterns is interesting, since the magnitude of λ is the outcome of the cumulative effect of t_r, ε_r, and $\acute{\varepsilon}_{II}$, in contrast to $\acute{\varepsilon}_{II}$ that is related to t_{II} only, which is highlighting the significance of λ concept. It has been proposed if the λ value is in the span of 1.5 to 2.5, the diffusion creep and power-law creep mechanisms have dominant effects on damage,[29] whereas any λ value greater than 2.5 means that necking takes the supremacy in the creep damage.[35] It is known that steels may have different values of λ for different creep conditions. The λ values of the CRT specimens that were calculated from eq. (1) are within the range of 2.05 to 2.33, and 2.22 in average.

Since the high temperature creep tests acquire shorter t_r, i.e., less creep strength in comparison to the low temperature creep tests, so it can be anticipated that λ varies inversely with t_r which is illustrated in Fig. 11(b). Moreover, it also demonstrates λ as inverse ductility factor with respect to rupture strength, since the λ decreases with increasing t_r. Additionally, the similarity of W_C, W_{II}, and 1/λ's finding for low and high creep temperatures, is heading to the fact of more energy accumulation for low temperatures specimens, hence resulting in low λ value than high temperatures consequently low temperatures specimens are more creep ductile. W_C and W_{II} should further be investigated for a large number of data sets to find their validity as it may contribute to the analysis of creep damage factors and mechanisms.

6. Conclusion

Creep rupture tests were conducted on the P91 samples for stress and temperature span of 155 MPa to 200 MPa; and of 640 °C (913K) to 675 °C (948 K) respectively for the prediction method development of creep rupture behavior. Microstructural investigations, hardness measurements, and fractographic analyses of the specimens showed that there is negligible microstructural degradation during creep rupture tests, and fracture surfaces have a clear ductile fracture appearance with the presence of dimples. The creep work density parameter based on the strain energy approach was derived and investigated via creep rupture test results at macro level. Some meaningful results and good correlations were observed, and various empirical equations were obtained from the creep parameters relations utilized in this manuscript such as percentage strain, steady state strain rate, rupture time, creep damage tolerance factor, and the creep work density. This experimental research highlighted the significance of the empirical analysis for P91 steel, which can be helpful in better understanding of the creep behavior. Current findings can also be used to elaborate the computational algorithms for the development of creep curves and creep life predictions.

Acknowledgment

This research work is conducted at Department of Metallurgical and Materials Engineering, METU, Ankara. The authors would like to thank Welding Technology and NDT Research/Application Center (METU, Ankara) officials, Dr. Koray Yurtisik and Murat Tolga Erturk for the arrangement of P91 material. Authors also extends acknowledgment for Dr. Onder Sahin and Huseyin Ceylan for their help in conducting creep rupture tests at Instron.

Nomenclature

CRT - Creep Rupture Test,
ε_o - Instantaneous creep strain,
ε_I - Primary creep strain,
ε_{II} - Steady state creep strain,
ε_{III} - Tertiary creep strain,
ε_r - Creep rupture strain,
$\%\varepsilon_I$ - Percent fraction of primary state creep strain,
$\%\varepsilon_{II}$ - Percent fraction of Steady state creep strain,
$\%\varepsilon_{III}$ - Percent fraction of tertiary state creep strain,
t_I - Time spent in primary creep region,
t_{II} - Time spent in secondary creep region,
t_{III} - Time spent in tertiary creep region,
t_r - Creep rupture time,
$\%t_I$ - Percent fraction of t_I,
$\%t_{II}$ - Percent fraction of t_{II},
$\%t_{III}$ - Percent fraction of t_{III},
$\acute{\varepsilon}_{II}$ - Strain rate in steady-state creep region,
$\acute{\varepsilon}_{avg}$ - Average strain rate,
E_c - Strain energy density,
W_c - Creep work density,
W_{II} - Work density for steady-state creep,
λ - Creep Damage Tolerance Factor

References

1. Council of The American Society of Mechanical Engineers, Rules for construction of Power Boilers (I), Nuclear Facility Components (III) & Pressure Vessels (VIII), 2015, 46 (2015).
2. V. K. Sikka and P. Patriarca, Analysis of weldment mechanical properties of modified 9 Cr-1Mo steel, Oak Ridge National Laboratory, Retrieved May 1, 1984 from https://inis.iaea.org/search/search.aspx?orig_q=RN:17007091.
3. S. Spigarelli, Int. J. Press. Vess. Pip., **101**, 64 (2013).
4. L. Maddi, D. Barbadikar, M. Sahare, A. R. Ballal, D. R. Peshwe, R. K. Paretkar, K. Laha and M. D. Mathew, Trans. Ind. Inst. Met., **68**, 259 (2015).
5. M. A. Abro and D. B. Lee, Coatings, **7**, 31 (2017).
6. M. Akhtar, A. Khajuria, M. K. Pandey, I. Ahmed and R. Bedi, Mater. Res. Express, **6,** 12 (2019).
7. J. P. Sanhueza, D. Rojas, J. Garcia, M. F. Melendrez, E. Toledo, C. Montalba, M. I. Alvarado and A. F. Jaramillo, Mater. Res. Express, **6**, 11 (2019).
8. M. A. Abro, J. Hahn and D. B. Lee, Korean J. Met. Mater., **57**, 236 (2019).
9. C. Pandey, Mater. Res. Express, **6**, 9 (2019).
10. M. Swei, A. S. Sedmak, B. Petrovski, Z. Z. Golubovi, S. A. Sedmak, M. Katini, and K. I. Azzab, Therm. Sci., **23**, 1203 (2019).
11. F. Vivier, C. Panait, A. F. Gourgues-Lorenzon and J. Besson, Proceedings of 17th European Conference on Fracture, p. 1095, Brno, Czech Republic (2008).
12. C. Panait, W. Bendick, A. Fuchsmann, A. F. Gourgues-Lorenzon and J. Besson, Int. J. Press. Vess. Pip., **87**, 326 (2010).
13. L. Huijun and D. Mitchell, Steel Res. Int., **84**, 1302 (2013).
14. Committee A01 of American Society for Testing and Materials, Standard Specification for Seamless Ferritic Alloy-Steel Pipe for High-Temperature Service (ASTM A335/A335M), **19**, 2 (2019).
15. C. Yunxiang, W. Yan, Hu. Ping, S. Yiyin and K. Yang, Acta Metall. Sin., **47**, 1372 (2011).
16. J. Besson, S. Leclercq, V. Gaffard and A. F. Gourgues-Lorenzon, Eng. Fract. Mech., **76**, 1460 (2009).
17. B. Wilshire and P. J. Scharning, Mater High Temp., 25, 55 (2014).
18. T. Masse and Y. Lejeail, Nucl. Eng. Des., **246**, 220 (2012).
19. K. Kimura, K. Suzuki, Y. Toda, H. Kushima and F. Abe, Proceedings of 28th MPA-NIMS Workshop on Safety and Availability in Energy Engineering, 2, p. 43, Stuttgart, Germany (2002).
20. A. Sedmak, M. Swei and B. Petrosvski, Fatig. Fract. Eng. Mater. Struct., **40**, 1267 (2017).
21. M. T. Whittaker and W. J. Harrison, Mater. High Temp., **31**, 233 (2014).
22. B. Wilshire and M. T. Whittaker, Acta Mater., **57**, 4115 (2009).
23. F. Dyson and T. B. Gibbons, Acta Metall, **35,** 2355 (1987).
24. A. Raj, N. Roy, B. N. Roy and A. K. Ray, High Temp. Mater. Processes (Berlin, Ger.), **34,** 731 (2015)
25. M. F. Ashby and B. F. Dyson, Proceedings of 6th International Conference on Fracture (ICF6), p. 3, New Delhi, India (1984).
26. M. J. Aslam and C. H. Gur, Proceeding of the 7th International Iron & Steel Symposium, p. 374, Izmir, Turkey (2019).
27. Committee E28 of American Society for Testing and Materials, Standard Test Methods for Conducting Creep, Creep-Rupture, and Stress-Rupture Tests of Metallic Materials (ASTM A139/ A139M), **11**, 4 (2018).
28. M. E. A. El-Azim, O. H. Ibrahim, O. E. El-Desoky, Mater. Sci. Eng., A, **560**, 678 (2013).
29. O. Nassif, T. J. Truster, R. Ma, K. B. Cochran, D. M. Parks, M. C. Messner and T.-L. Sham, Model. Simulat. Mater. Sci. Eng., **27**, (2019).
30. B. K. Choudhary and I, S. Edwin, J. Nucl. Mater., **412**, 82 (2011).
31. V. Gaffard, PhD Thesis, p. 161, Paris School of Mines, Paris (2004).
32. K. Kimura, H. Kushima, K. Sawada, Mater. Sci. Eng., A, **510-511**, 58 (2009).
33. T. Shrestha, M. Basirat, I. Charit, G. P. Potirniche and K. K. Rink, Mater. Sci. Eng., A, **565**, 382 (2013).
34. L. An, Q. Xu, D. Xu and Z. Lou, Proceeding of the 10th International Conference on Science Computing, p. 184, Las Vegas, USA (2013).
35. B. K. Choudhary, C. Phaniraj and B. Raj, Tran. Ind. Inst. Metals, **63**, 675 (2010).

Author Information

Muhammad Junaid Aslam

Department of Metallurgical and Materials Engineering, Middle East Technical University, Ankara, Turkey

Cemil Hakan Gur

Professor (Chair), Department of Metallurgical and Materials Engineering, Middle East Technical University, Ankara, Turkey.

Director, Welding Technology and NDT Research/ Application Center, Middle East Technical University, Ankara, Turkey